Component-Level Reliability Assessment of a Direct-Drive PMSG Wind Power Converter Considering Two Terms of Thermal Cycles and the Parameter Sensitivity Analysis

Shuaichen Ye, *Student Member, IEEE*, Dao Zhou, *Senior Member, IEEE*, Xiaoxian Yao, and Frede Blaabjerg, *Fellow, IEEE*

***Abstract*—The availability and efficiency of a wind power system are highly affected by the failure or the unreliable operation of its power converter. This article investigates the failure rate and annual consumed lifetime for a 2-MW direct-drive permanent magnet synchronous generator based full-scale converter in a wind power generation system. The reliability assessment mainly focuses on the component level, namely, diodes and IGBTs, in both of the machine-side converter and the grid-side converter. Annual damages and power cycles for semiconductors are calculated separately under long-term thermal cycles (several seconds to hours) and short-term thermal cycles (dozens to hundreds of milliseconds). Experiments regarding thermal stress measuring for different semiconductors under short-term thermal cycles are affiliated. A comparison between different thermal cycles is given and discussed in detail. To ensure a visualized time-to-failure evaluation, a Monte Carlo method is used to generate the lifetime distributions and entire unreliability functions for power semiconductors. Final B_{10} and B_1 lifetimes can easily be observed from the cumulative distribution functions. Moreover, different standard deviations are assumed for parameters in the Bayerer's lifetime model, and by using several parallel Monte Carlo algorithms, parameter sensitivity to the final lifetime evaluation is analyzed.**

***Index Terms*—Bayerer's lifetime model, component-level reliability, Monte Carlo method, parameter sensitivity, permanent magnet synchronous generator (PMSG), thermal cycles, wind power system.**

I. Introduction

RECENTLY, the usage of the full-scale power converter in wind power generation systems has been increasing steadily [1], [2]. Compared with the partial-scale power converter, the main advantage of the full-scale power converter lies in its adaptability to the upgraded grid codes [3]. A major category for the full-scale power converter is associated with the permanent magnet synchronous generator (PMSG), which eliminates the slip rings and supports the grid operation better.

To obtain optimal wind conditions, wind turbines are normally installed in remote areas, such as an offshore wind farm. Due to the high maintenance cost, the lifespan and reliability of the wind power system attract increasing concerns from wind turbine manufacturers. According to a survey in [4], the power electronics part seems to have the highest failure rate among all subsystems, such as the turbine, the generator, and the control circuit. Moreover, based on investigations in [5], [6], the thermal stress is one of the most critical failure inducements for a power module in the wind generation system, among the elements such as the humidity, the pollution, and the mechanical vibration. Although according to surveys given by Fischer [7], [8], condensation and environmental humidity dominate in the incidence of liquid-cooled converter breakdowns, it has no sufficient evidence to reveal that these stressors also play the core role in the air-cooled converter, which is the cooling strategy employed in this article. Hence, it still has some practical significations to investigate the power module reliability with respect to the thermal stress.

Generally, the power converter reliability is mainly evaluated according to the long-term thermal cycles [9]. As shown in Fig. 1, the cycle period for the long-term thermal stress is usually from several seconds to hours. The wind-speed and the ambient temperature are regarded as constant during each single period, and they are assumed to vary only at different sampling points in a step manner. However, although the sampling time is short, non-negligible high-frequency junction temperature fluctuations still exist on the chip of the power module in both of the machine-side converter (MSC) and the grid-side converter (GSC). They are introduced by the alternating current through the power converter, which leads to the conduction of power components with a 50% duty cycle. Period of this kind of thermal stress is defined as short-term cycle, and its scale is determined by the fundamental stator current frequency of the PMSG for the MSC and by the grid current frequency for the GSC. Therefore, the only calculation of the long-term thermal cycles is not enough.

Manuscript received August 20, 2020; revised December 23, 2020 and February 24, 2021; accepted March 1, 2021. Date of publication March 8, 2021; date of current version June 1, 2021. Recommended for publication by Associate Editor A. J. Marques Cardoso. *(Corresponding author: Dao Zhou.)*

Shuaichen Ye and Xiaoxian Yao are with the School of Aerospace Engineering, Beijing Institute of Technology, Beijing 100081, China (e-mail: yesc_bit@163.com; yxx11@bit.edu.cn).

Dao Zhou and Frede Blaabjerg are with the Department of Energy Technology, Aalborg University, 9220 Aalborg, Denmark (e-mail: zda@et.aau.dk; fbl@et.aau.dk).

Color versions of one or more figures in this article are available at https://doi.org/10.1109/TPEL.2021.3064363.

Digital Object Identifier 10.1109/TPEL.2021.3064363

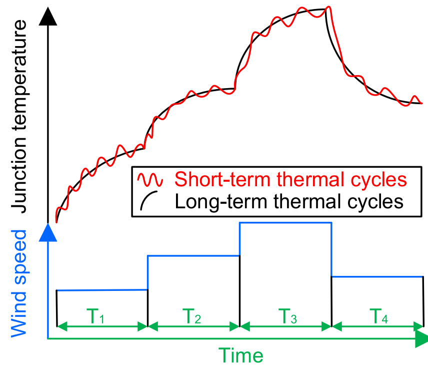

Fig. 1. Concept of long-term and short-term thermal cycles under a random wind profile.

Although the resolution of the wind mission profile has been reduced to at least 1 s in [10]–[13] for the reliability assessment of both the full-scale and the partial-scale power converters, they were still long-term calculations inherently and cannot reflect the damage performance under short-term thermal stress, whose frequency is usually from several to dozens of Hz. In other words, the calculation of the short-term thermal stress cannot be realized merely by improving the sampling resolution of the annual wind speed profile, it should be calculated under different wind speeds in a paralleled manner considering their annual distributions. In [14]–[16], the basic strategy of the short-term reliability assessment has been introduced, but they mainly focused on the thermal stress comparisons among different constant wind speeds. The actual wind circumstance and the lifetime model need to be considered and integrated from the consumed lifetime calculation point of view. Moreover, [17] and [18] presented thorough calculation flowcharts of the annual consumed lifetime (ACL) under short-term cycles for the PMSG- and the DFIG-based wind power converters, respectively, but the discrete wind profile was neglected and in [17] only the MSC was considered. Thus, the damage caused by the long-term thermal cycles was excluded on the contrary, which still worsen the accuracy of the lifetime estimation, and the reliability for the entire back-to-back (BTB) full-scale power converter requires a further research. Some recent studies [6], [19] have also addressed both of the long-term and the short-term thermal cycles in the power semiconductor loss calculation, but the thermal characteristic under short-term cycles is just taken as the auxiliary and no explicit comparison was made between the results of these two thermal cycles under the same wind profile. So, it is still unclear which of these two thermal cycles dominates in the power converter failure mechanism. Besides, to achieve a more accurate component-level reliability assessment in the power converter, final lifetimes of semiconductors should be calculated as an accumulation of the results under both the long-term and the short-term thermal cycles, which was ignored universally in previous researches. Thus, the first aim of this article is to compare the ACL of power semiconductors between operating under long-term and short-term thermal cycles and to analyze the internal inducements of the result differences for both of the MSC and the GSC.

Although an accumulative damage and a lifetime can be obtained via the aforementioned calculation, because the failure data provided by the manufacturer is insufficient, this process can only obtain the B_X lifetime of the semiconductor (B_X lifetime is a percentile lifetime, which is defined as a measurement of the time by which X% of a population of semiconductors have failed), such as B_{10} lifetime in this article [20], [21]. As indicated in [22], B_X lifetime is revealed as a specific point on the entire reliability profile, which can only reflect the time-to-failure characteristic of the most fragile power component rather from the global point of view. The overall failure tendency profile for the individual power component still needs to be generated using a Monte Carlo method. Hence, the component-level reliability can be assessed in a more visualized manner and a stricter B_1 lifetime can be subsequently observed [23].

In the overall reliability profile evaluation process, a lifetime model such as the Bayerer' model [24] or the Coffin–Manson model [25] is first employed. Then, based on the manufacturing deviation and the environment uncertainties, practical parameter variations in the lifetime model are introduced, and normal distributions are assumed for all uncertain parameters. By integrating all the parameter uncertainties into the lifetime model, numerous lifetime points can be sampled by the Monte Carlo algorithm [26]. Afterwards, by fitting these points into the Weibull distribution, an entire reliability (or unreliability) profile can be generated by accumulation. To unify the calculation, the standard deviation in normal distributions for uncertain parameters is chosen as a fixed value, such as 5% in [27], [28]. However, influences of these parameters to the final lifetime are seldom focused, which is an essential reference to the power converter manufacturing procedure. In this article, the Bayerer's lifetime model is taken as an example and the parameter sensitivity is analyzed by setting a series of variation percentage to all parameters. Some corresponding comparative calculations are given to reveal effects of different parameter deviations to the final component reliability.

The reminder of this article is arranged as follows. Sections II and III introduce the power component lifetime evaluation process under long-term and short-term thermal cycles, respectively. Some steady-state thermal measurements regarding different operation modes of semiconductors are also presented in Section III. Section IV presents a comparison of results obtained in Sections II and III as well as some relevant discussions. Section V generates the entire reliability profiles for diode and IGBT via the Monte Carlo algorithm. Section VI investigates the parameter sensitivity of the Bayerer's lifetime model from the semiconductor reliability point of view. Finally, Section VII concludes this article.

II. Reliability Evaluation of Semiconductors Under Long-Term Thermal Cycles

An overall configuration of the PMSG-based wind power generation system is shown in Fig. 2. It can be seen that a full-scale BTB power converter consists of an MSC and a GSC, which are connected via a dc-link capacitor bank for decoupling. Besides, a filter is applied to eliminate the PWM

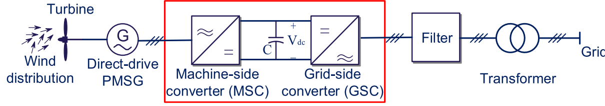

Fig. 2. Overall direct-drive PMSG-based wind power generation system.

TABLE I
PARAMETERS OF THE WIND TURBINE

Parameters	Values
Blade radius (m)	41.3
Cut-in wind speed (m/s)	3
Rated wind speed (m/s)	12
Cut-off wind speed (m/s)	25
Optimal tip speed ratio	8.1
Maximum power coefficient	0.41
Range of turbine angular speed (rpm)	6-18

TABLE II
PARAMETERS FOR THE DIRECT-DRIVE PMSG AND THE MSC

Parameters	Values
Rated power (MW)	2.0
Rated stator voltage (V)	477
Rated stator current (A)	3302
Stator current frequency range (Hz)	2.6-7.8
Maximum rotor angular speed (rpm)	18
Minimum rotor angular speed (rpm)	6
Number of pole pairs	26
Rated rotor flux linkage (Wb)	5.826 (rms)
Stator resistance (mΩ)	0.831
Stator inductance (mH)	1.573
DC-link voltage (V)	1100
Switching frequency (kHz)	2
Rated parameter of power module	1 kA/1.7 kV
MSC structure	4 modules in parallel

harmonics and a transformer is used to step up the grid voltage to the transmission level. This article mainly focuses on the semiconductor reliability analysis of the MSC and the GSC, which share the same scale of the input power. As a case study, a direct-drive 2-MW PMSG wind turbine system is investigated [29], [30], and detailed specifications for each subsystems are listed in Tables I–III.

The wind speed and the ambient temperature are sampled every 1 h during 1 year. An overall flowchart for the power semiconductor B_{10} lifetime evaluation in the BTB converter is illustrated in Fig. 3.

For the MSC calculation, the turbine model can link the relationship between the wind speeds to the output power, which is illustrated in Fig. 4(b). Together with the PMSG and the converter models, the voltage and the current of the converter can be calculated at various wind speeds as shown in Fig. 4(c) and

TABLE III
PARAMETERS FOR THE GSC

Parameters	Values
Rated power (MW)	2.0
Grid voltage (V)	563
Rated grid current (A)	2321
Grid current frequency (Hz)	50
Switching frequency (kHz)	2
Filter inductance (mH)	0.5
Rated parameter of power module	1 kA/1.7 kV
GSC structure	4 modules in parallel

(d), respectively. On the basis of calculating the displacement angle, the switching loss and conduction loss of the diode and IGBT can be obtained by loss model according to the following equations [31]:

$$P_{\text{con_diode}} = V_f\left(\frac{I_s}{4}\right)\left(\frac{1}{2\pi} - \frac{1}{8}\frac{U_s}{U_{\text{dc}}}\cos\varphi\right) + R_f\left(\frac{I_s}{4}\right)^2\left(\frac{1}{8} - \frac{1}{3\pi}\frac{U_s}{U_{\text{dc}}}\cos\varphi\right) \quad (1)$$

$$P_{\text{con_IGBT}} = V_{\text{ce}}\left(\frac{I_s}{4}\right)\left(\frac{1}{2\pi} + \frac{1}{8}\frac{U_s}{U_{\text{dc}}}\cos\varphi\right) + R_{ce}\left(\frac{I_s}{4}\right)^2\left(\frac{1}{8} + \frac{1}{3\pi}\frac{U_s}{U_{\text{dc}}}\cos\varphi\right) \quad (2)$$

$$P_{\text{sw_diode}} = f_{\text{sw}}\left(\frac{A_{\text{diode}}}{2} + \frac{B_{\text{diode}}}{\pi}\left(\frac{I_s}{4}\right) + \frac{C_{\text{diode}}}{4}\left(\frac{I_s}{4}\right)^2\right) \times \frac{U_{\text{dc}}}{1000} \quad (3)$$

$$P_{\text{sw_IGBT}} = f_{\text{sw}}\left(\frac{A_{\text{IGBT}}}{2} + \frac{B_{\text{IGBT}}}{\pi}\left(\frac{I_s}{4}\right) + \frac{C_{\text{IGBT}}}{4}\left(\frac{I_s}{4}\right)^2\right) \times \frac{U_{\text{dc}}}{1000} \quad (4)$$

where P_{con} represents conduction loss, P_{sw} represents switching loss, subscript "diode" means the calculation result for diode, subscript "IGBT" means the calculation result for IGBT, U_s is the stator voltage, I_s is the stator current, f_{sw} is the switching frequency, U_{dc} is the dc-link voltage, and φ is the displacement angle between the stator voltage and the stator current, coefficients used in (1) to (4) are listed as Table IV. The total dissipations of the components [Fig. 4(e)] can be obtained by summing their switching loss and conduction loss. Combined with the real-time ambient temperature, the junction temperature of each component [Fig. 4(f)] is estimated from the thermal models. In the thermal model, thermal impedances of power semiconductors and an air-cooling system are considered with a Foster structure preferred by industrial applications [32]. Key thermal specifications are shown in Table V.

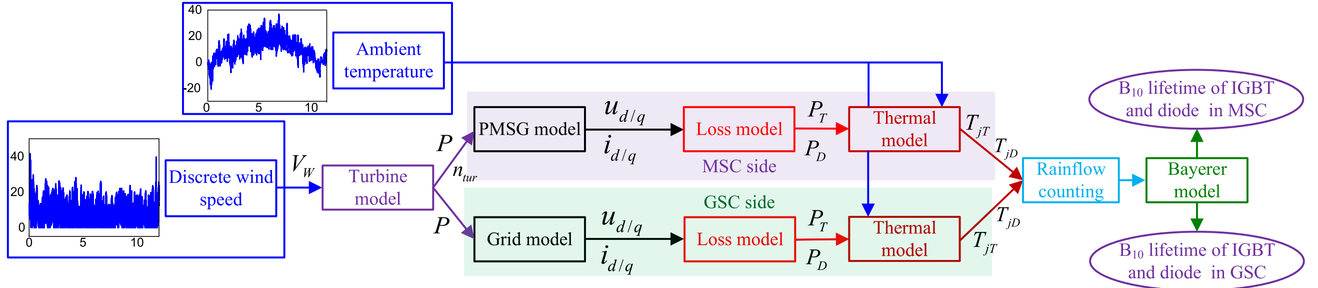

Fig. 3. Flowchart to calculate B_{10} lifetime of IGBT and diode under real-time wind speed and ambient temperature.

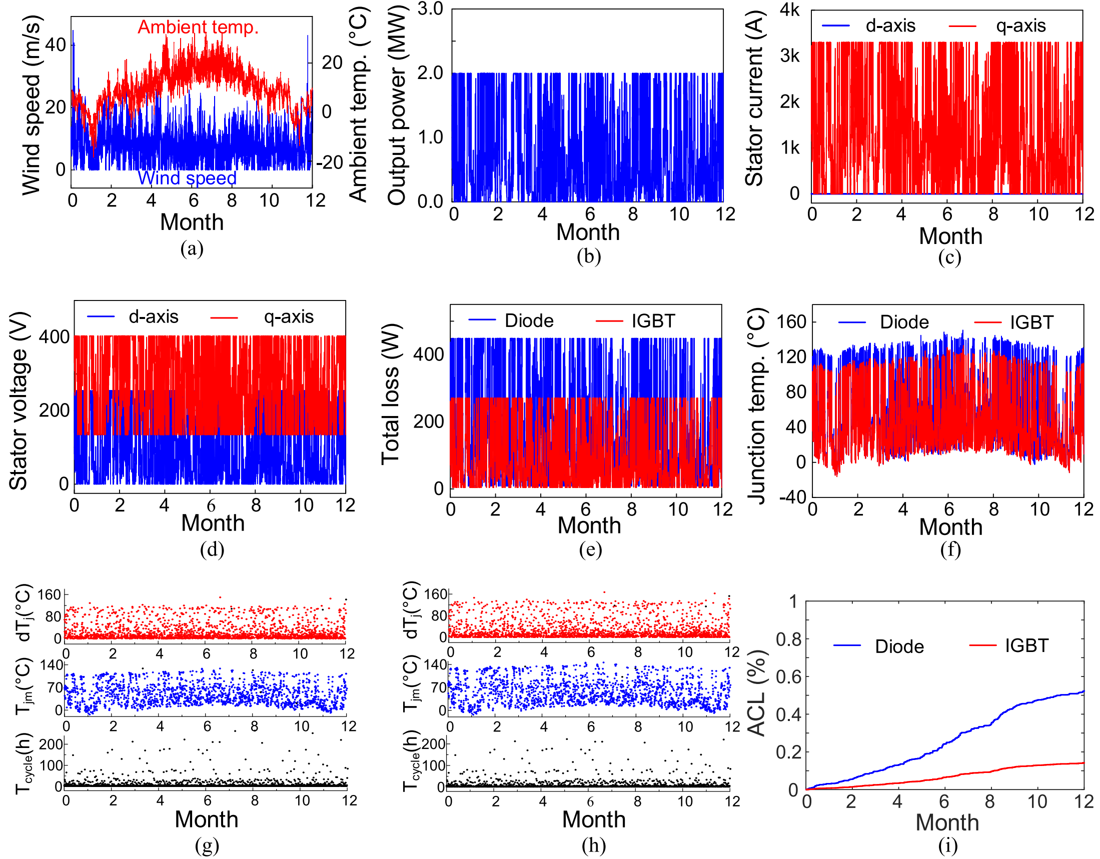

Fig. 4. Results of long-term thermal cycle based lifetime estimation for the MSC. (a) Wind speed and ambient temperature. (b) Turbine output power. (c) PMSG stator current in *d-q* coordinate frame. (d) PMSG stator voltage in *d-q* coordinate frame. (e) Total loss for diode and IGBT. (f) Junction temperature for diode and IGBT. (g) and (h) Rainflow counting results for diode and IGBT (from top to bottom: junction temperature fluctuation, mean junction temperature, and thermal cycle period). (i) Annual consumed lifetime (ACL) for diode and IGBT.

Then, the irregular thermal profiles of the IGBT and diode the can be extracted using the Rainflow counting algorithm, so corresponding mean junction temperatures, junction temperature fluctuations, and thermal cycle periods are obtained. In Fig. 4(g) and (h), Rainflow counting results for IGBT and diode are presented, respectively. There are 1980 total thermal cycles in both of the IGBT and the diode counting results during 1 year. However, the mean junction temperatures of the diode are much larger than that of the IGBT, which is mainly caused by the smaller chip size of the diode. Following this, the B_{10} lifetime of diode and IGBT can be calculated using the Bayerer's lifetime model [33], and the annual damage of them can be obtained by accumulating B_{10} lifetime, which is shown in Fig. 4(a). It illustrates that the ACL of diode is 0.52%, which is almost four times to the 0.14% of IGBT.

For the GSC calculation, the key difference lies in the replacement of the PMSG model by the GSC model, which has an opposite *d–q* axis definition regarding the current and the voltage calculation compared with the MSC. Voltage and current vectors of the GSC can be expressed as follows:

$$\boldsymbol{i} = i_{gd} + j \cdot i_{gq} \tag{5}$$

$$\boldsymbol{u} = U_g + 2\pi f_g L_g \cdot i_{gq} + j \cdot 2\pi f_g L \cdot i_{gd} \tag{6}$$

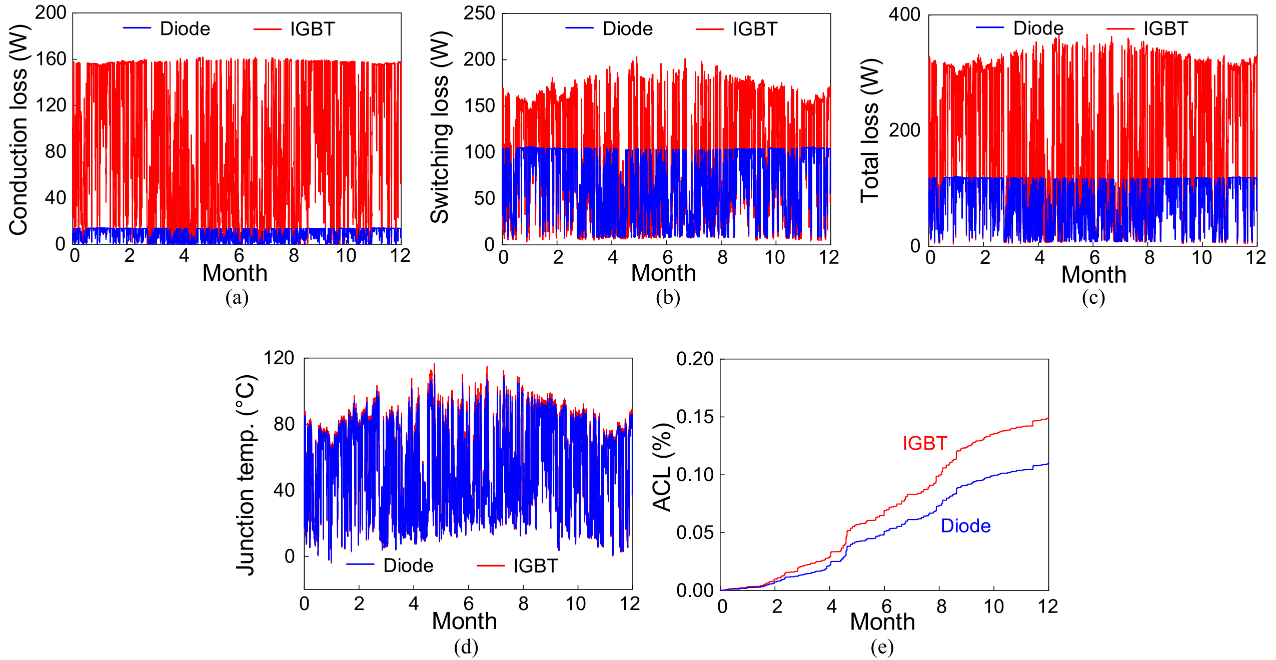

Fig. 5. Results of long-term thermal cycle based lifetime estimation for the GSC. (a) Conduction loss for diode and IGBT. (b) Switching loss for diode and IGBT. (c) Total loss for diode and IGBT. (d) Junction temperature for diode and IGBT. (e) ACL for diode and IGBT.

TABLE IV
COEFFICIENTS USED IN THE LOSS MODEL

Parameters	Values	Parameters	Values
V_f (1 kA/150 °C)	0.66	B_{diode}	0.35
V_{ce} (1 kA/150 °C)	0.67	C_{diode}	-1.20E-4
R_f (1 kA/150 °C)	1.13E-3	A_{IGBT}	32.85
R_{ce} (1 kA/150 °C)	1.64E-3	B_{IGBT}	0.47
A_{diode}	9.14	C_{IGBT}	2.81E-4

where subscript "*d*" and "*q*" represent values under *d*- and *q*-axis, respectively; U_g, f_g, and L_g are the grid phase voltage, the grid current, and the filter inductance, respectively, as given in Table III. Thus, with a similar process, the power losses, junction temperatures, and ACLs for the diode and the IGBT in GSC can be illustrated as Fig. 5.

It can be observed from Fig. 5(a) and (b) that the conduction and the switching losses of the IGBT are much higher than those of the diode, which induces a corresponding higher total loss in Fig. 5(c) and a shorter ACL of the IGBT in Fig. 5(e). This phenomenon differs from the loss condition of the MSC component, where the total loss of the diode dominates [as presented in Fig. 4(e)]. This is because the GSC operates in an inverter mode, where the conducting and the frequent switching operations of the IGBT prevail during the entire working stage. While for the MSC, a rectifier mode is required, where long-time conducting of the diode produces a higher loss and a larger junction temperature.

III. Reliability Evaluation of Semiconductors Under Short-Term Thermal Cycles

A. Analytical Calculation

According to the specifications given in Tables I–III, frequencies of short-term thermal cycles are maximum 7.8 Hz for the MSC and 50 Hz for the GSC. As a relatively long period (1 h in this case) is selected to sample the real-time wind speed and ambient temperature, the thermal dissipation and accumulated damage caused by short-term thermal cycles cannot be reflected from the aforementioned long-term calculation. Considering the stator current frequency of the PMSG is decided by the real-time wind speed indirectly, the annual wind speed in Fig. 3 should be sorted by the Weibull distribution. Besides, to obtain the same comparative and subsequent summing conditions, the reliability evaluation under short-term thermal cycle shares the same group of the key parameters with that in the long-term thermal cycle based evaluation. A flowchart of lifetime calculation for the power semiconductors in both the MSC and GSC under the Weibull wind speed distribution is shown in Fig. 6.

In the calculation process of the MSC, the input Weibull speed distribution is a statistical result generated from the annual real-time wind speed. In this distribution, the lowest speed is the same as turbine cut-in speed of 3 m/s and the highest speed is the same as the turbine cut-off speed of 25 m/s, from the lowest to the highest speed, a resolution of 1m/s is selected to obtain 23 discrete statistical speed results. By dividing the total wind speed sampling amounts with each statistical speed results, the proportion factor for each speed value can be obtained, which will be used for subsequent accumulation. Calculation results of

TABLE V
KEY PARAMETERS USED IN THE THERMAL MODEL [9]

	Diode		IGBT		Air cooling system	
Thermal resistance (°C/kW)	1st layer	0.48E-3	1st layer	0.30E-3	1st layer	6.60E-3
	2nd layer	3.61E-3	2nd layer	1.60E-3		
	3rd layer	3.46E-2	3rd layer	1.80E-2	2nd layer	1.95E-2
	4th layer	6.47E-3	4th layer	3.10E-3		
Thermal time constant (s)	1st layer	1.80E-4	1st layer	3.00E-4	1st layer	17.93
	2nd layer	8.90E-4	2nd layer	1.30E-3		
	3rd layer	3.00E-2	3rd layer	0.04	2nd layer	5.27
	4th layer	2.00	4th layer	0.40		

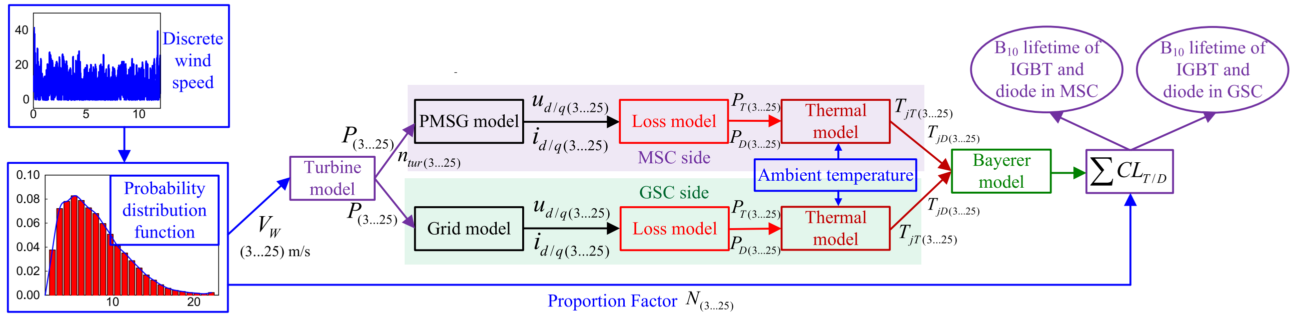

Fig. 6. Flowchart to calculate B_{10} lifetimes and accumulated damages of IGBT and diode under Weibull wind speed distribution.

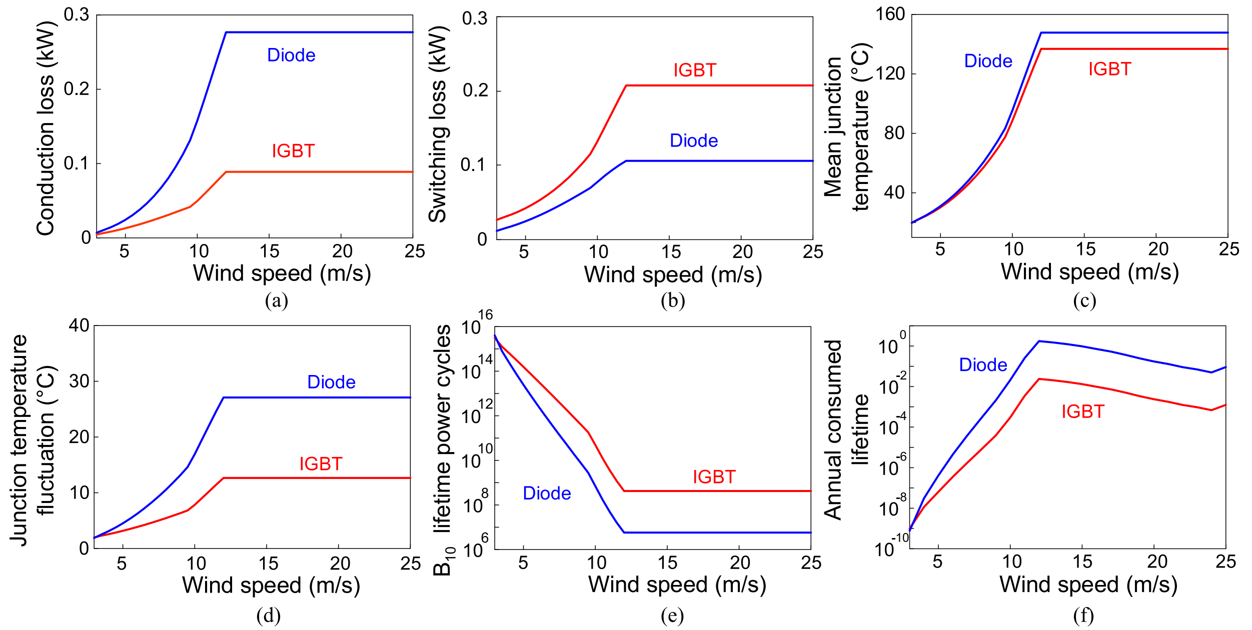

Fig. 7. Calculation results of short-term thermal cycle based lifetime estimation for the MSC. (a) Conduction loss for diode and IGBT. (b) Switching loss for diode and IGBT. (c) Mean junction temperature for diode and IGBT. (d) Junction temperature fluctuation for diode and IGBT. (e) B_{10} lifetime power cycles for diode and IGBT. (f) ACL for diode and IGBT.

thermal stresses and consumed lifetimes for semiconductors in the MSC are shown in Fig. 7.

In general, the calculation procedure under short-term thermal cycles is similar to that under long-term cycles. First, a relationship between the turbine output power and the wind speed is established using the turbine model, and the discrete stator currents and voltages for each wind speed can be obtained via the PMSG d–q frame model. Then, the total loss dissipations of diode and IGBT, which include conduction loss of Fig. 7(a) and switching loss of Fig. 7(b), can be calculated from the loss model.

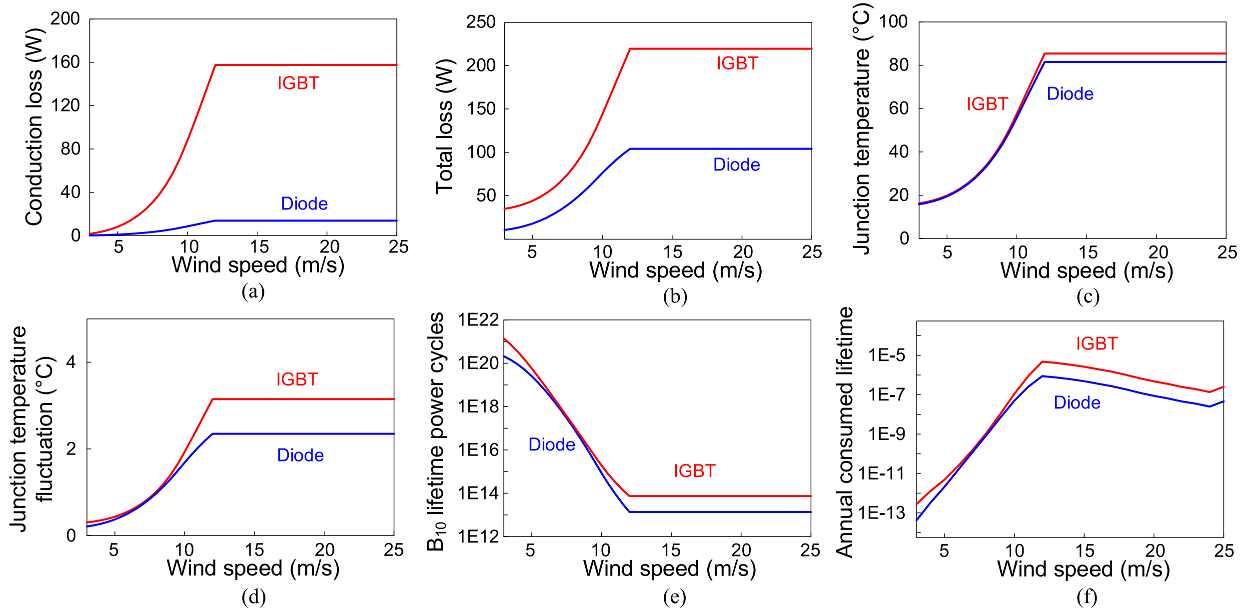

Fig. 8. Calculation results of short-term thermal cycle based lifetime estimation for the GSC. (a) Conduction loss for diode and IGBT. (b) Switching loss for diode and IGBT. (c) Mean junction temperature for diode and IGBT. (d) Junction temperature fluctuation for diode and IGBT. (e) B_{10} lifetime power cycles for diode and IGBT. (f) ACL for diode and IGBT.

Further, thermal profiles of semiconductors, which include the mean junction temperature and the junction temperature fluctuation, can be illustrated by the thermal model. Afterwards, based on a Bayerer's model, total power cycles or B_{10} lifetimes of diode and IGBT under different wind speeds are calculated as Fig. 7(e). Finally, the accumulative annual damage of diode and IGBT can be estimated according to different wind speeds in Fig. 7(f).

However, the major difference between the calculations under these two categories of thermal cycles lies in the obtaining of mean junction temperature and junction temperature fluctuation. For the lifetime calculation under long-term thermal cycles, the mean junction temperature and the junction temperature fluctuation are hard to be estimated directly from the annual discrete junction temperature profile, which leads to employment of a Rainflow counting algorithm. However, for short-term thermal cycle, which assumes the wind speed as a discrete constant value during one year, the thermal characteristics of the semiconductors with the Foster structures can be directly calculated from following [34]:

$$T_{jm_\text{diode/IGBT}} = P_{\text{diode/IGBT}} \left(\sum_{i=1}^{m} R_{\text{th_diode/IGBT}}(i) + \sum_{i=1}^{n} R_{\text{th_}c}(i) \right) + T_a \quad (7)$$

$$dT_{j_\text{diode/IGBT}} = 2P_{\text{diode/IGBT}} \times \sum_{i=1}^{m} \left(R_{\text{th_diode/IGBT}}(i) \frac{\left(1 - e^{\frac{-t_{\text{on}}}{\tau_{\text{diode/IGBT}}(i)}}\right)^2}{1 - e^{\frac{-1/f_e}{\tau_{\text{diode/IGBT}}(i)}}} \right) \quad (8)$$

where T_{jm} represents mean junction temperature, dT_j represents junction temperature fluctuation, i is the ith Foster layer, m is the total layers for semiconductors, n is the total layer for air-cooling system, P is the total power loss for each semiconductor, T_a is the constant ambient temperature, which is chosen as the mean value of an annual temperature profile presented in Fig. 4(a), t_{on} is the ON-state time for each semiconductor, f_e is the current frequency, R_{th} and τ denote thermal resistance and thermal time constant, respectively, as shown in Table V.

Moreover, by employing a similar procedure but with specifications of grid voltage and current, thermal stresses and lifetimes for GSC power component can be evaluated and illustrated in Fig. 8. It is clearly observed that, compared with Fig. 7, the phenomenon of the IGBT loss dominating still exists under the inverter mode, which is in consistent with the result obtained from the long-term thermal cycle based evaluation.

Additionally, it is noteworthy that for all evaluations under different thermal cycles, following assumptions are universally suitable.

1) A unified failure mechanism exists in all Foster layers, which means the soldering cracks are neglected between different layers [32].
2) The fatigue damage accumulates in a linear manner, which obeys the Miner's rule [35].
3) Parameters in the Bayerer's lifetime model are constant during the B_{10} lifetime calculation.

B. Experimental Validation

To reveal thermal stresses of the diode and IGBT under different operation modes of the converter with short-term thermal cycles, experiments were performed using an H-bridge module

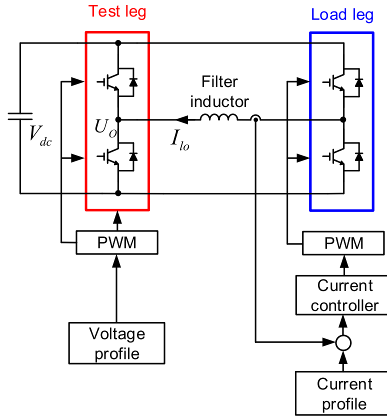

Fig. 9. Circuit configuration of H-bridge module.

with two legs under a lower power level. The circuit configuration of the H-bridge and its control strategy are shown in Fig. 9. In this setup, the dc-link voltage is 400 V, the peak loading current is 20 A, and a 300 μH filter inductor is equipped in between the loading leg and the test leg to enable the switchable operation of the H-bridge. It is noteworthy that the operation modes of the test leg can be altered by changing the direction of the loading current I_{lo} via a current controller. For the rectifier mode, which emulates the operation of the MSC, the loading current is in phase with the output voltage U_o. While for the inverter mode, which emulates the operation of the GSC, a half-period phase difference exists between I_{lo} and U_o.

Some comparative simulations are carried out to indicate the equivalence between the PMSG-based wind power system and the configured H-bridge module. The purpose of this comparison is to reveal that the H-bridge module can totally emulate the operation conditions of both the MSC and the GSC. According to [36], loading and thermal behaviors of one power semiconductor are determined by its dominant factors, such as the fundamental frequency, the current amplitude, the dc-link voltage, the modulation index, and the displacement angle. As long as the H-bridge circuit can achieve the identical aforementioned parameters with the PMSG power converter, it can be assumed that the thermal stress of the power semiconductor behaves similarly. However, as the power rating of the H-bridge system is a scaling down comparing with the BTB converter in the wind power system, their current and voltage amplitudes cannot be the same. Thus, the per-unit (p.u.) value is used as a replacement, which is defined as the ratio between the phase voltage/current to the rated voltage/current. Specifically, rated values for the wind power converter are included in Tables II and III. It can be observed from Fig. 10 that by adjusting the reference current, modulation index, and fundamental frequency, circuit factors (including the p.u. values and the displacement angle) of the testing leg in the H-bridge is in accordance with that of the power converter under different power levels (i.e., full-load, half-load, and quarter-load). Therefore, it is evident that the configured H-bridge module can emulate the loss profile and thermal stress of both the MSC and the GSC under the component level.

Corresponding to the circuit configuration, a DSP TMS320F28335 controller based experimental platform is constructed and shown in Fig. 11. In this setup, the PWM signals are produced by the ePWM module with a rated switching frequency of 10 kHz. For the junction temperature measurement, as the fundamental frequency of the loading current is 10 Hz, a high-frequency temperature fluctuation will also emerge, measuring equipment with a rapid response is therefore required. The OTG-F fiber optic thermometer with a 5 ms response time and its corresponding monitoring system produced by OpSens [37] are selected as the measuring tool in this experiment. During the testing, the probe of the thermometer needs to contact the chip surface of the semiconductor. Unlike the measuring scheme with the thermographic camera, the fiber optic thermometer can reserve the dielectric gel of the power module, which ensures the effective voltage isolation.

Fig. 12 exhibits steady-state chip junction temperature profiles for the diode and the IGBT under different operation modes. It can be observed that, under the rectifier mode in Fig. 12(a), the mean junction temperature and the junction temperature fluctuation of the diode are both higher than those of the IGBT. This means the diode is more stressed, which corresponds to the results for MSC given in Fig. 7(c) and (d). While for the inverter mode in Fig. 12(b), the IGBT is more stressed, which also agrees with the results for GSC in Fig. 8(c) and (d).

IV. Comparison Between Long-Term and Short-Term Thermal Cycles

Based on the ACL calculation with long-term thermal cycles in Figs. 4 and 5 and short-term thermal cycles in Figs. 7 and 8, the total consumed lifetime (TCL) of the power semiconductors can be compared. It is noted that, for the long-term thermal cycle based evaluation, the semiconductor TCL in the MSC and GSC is same as the results obtained in Fig. 4(i) and Fig. 5(e), respectively. However, in Fig. 7(f) and Fig. 8(f), the short-term thermal cycle based evaluation contains all the consumed lifetime results under different wind speeds, which should be added after multiplying by their proportions in the annual wind speed profile. The comparative results of TCL for the diode and IGBT with different thermal cycles are shown in Fig. 13.

From the comparison, following phenomena can be observed.

1) In the MSC, the TCL for diode are higher than that of the IGBT for both thermal cycles, because a higher total loss is produced on the diode chip in the rectifier mode. While in the GSC, the TCL for IGBT dominates, but the TCL gaps between two kinds of semiconductors are reduced compared with the MSC. This is because although more losses are produced on the IGBT chip in the inverter mode, due to its larger chip size, a superior cooling performance can prevent an obvious increasing of the junction temperature as well as the TCL.
2) In the MSC, the evaluated TCL of diode under short-term thermal cycles is much higher than the result obtained under long-term thermal cycles, while for the IGBT, the TCL with long-term thermal cycles takes a major proportion. In the GSC, for both semiconductors, the TCL under long-term thermal cycles dominates.
3) Due to the GSC has a higher current frequency compared with the generator stator, chip junction temperature

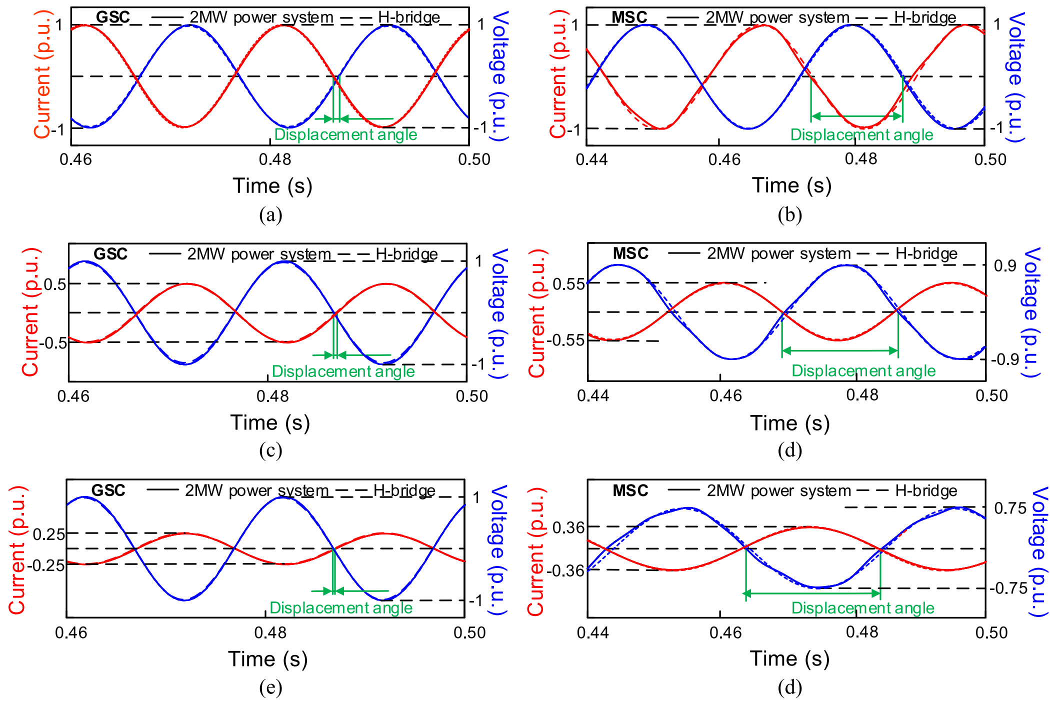

Fig. 10. Circuit behavior emulations of the H-bridge module to the BTB converter in the wind power system under the full-load operation of (a) inverter mode (GSC) and (b) rectifier mode (MSC); under the half-load operation of (c) inverter mode (GSC) and (d) rectifier mode (MSC); and under the quarter-load operation of (e) inverter mode (GSC) and (f) rectifier mode (MSC).

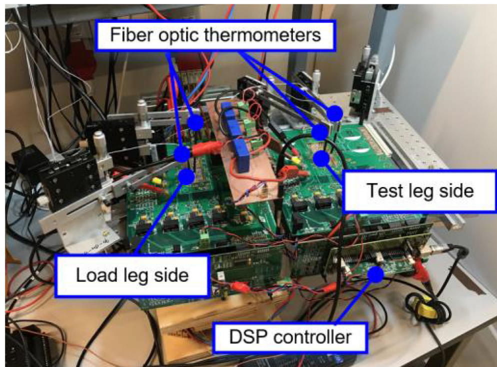

Fig. 11. Experimental platform.

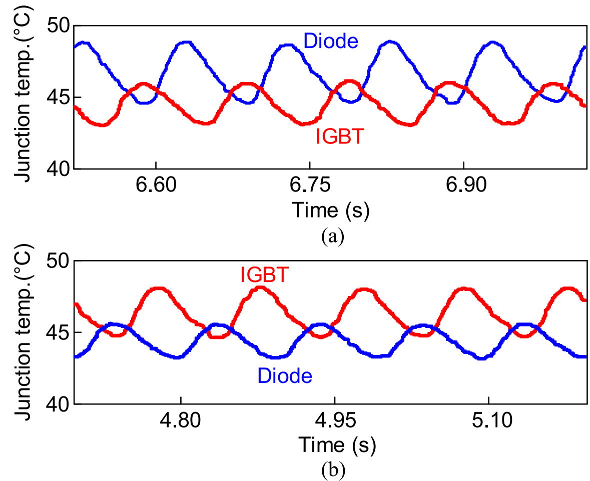

Fig. 12. Measured steady-state chip junction temperatures for power semiconductors under (a) rectifier mode (MSC) and (b) inverter mode (GSC).

fluctuations for the GSC are much lower [as presented in Fig. 8(d)], and further induces lower TCLs under the short-term thermal cycle based evaluation, which are two orders of magnitude smaller than those under the long-term thermal cycle based evaluation (comparing 2.26E-3 to 0.15 for IGBT and 4.26E-4 to 0.11 for diode).

Therefore, some suggestions can be made for the practical design of the power converter and assessment of existing wind generation systems. For example, lifetime expectancy for the diode with short-term thermal cycles and for the IGBT with long-term thermal cycles should be given more emphasis during failure mechanism analysis in the MSC. Besides, for the GSC with a high current frequency, only TCL under long-term thermal cycles requires attention for reliability assessment.

V. Component-Level Reliability Profiles for MSC and GSC

For the aforementioned calculations, only B_{10} lifetimes for the individual diode or IGBT are focused, which can only reflect the lifetime when 10% semiconductors fail in a BTB converter. However, for a complex system with multiple converters in parallel, the B_{10} lifetime is not sufficient to reveal its reliability and a stricter B_1 lifetime or the entire reliability distribution profile is preferred. To obtain the entire lifetime profile for power components, uncertainties and variations for parameters in the

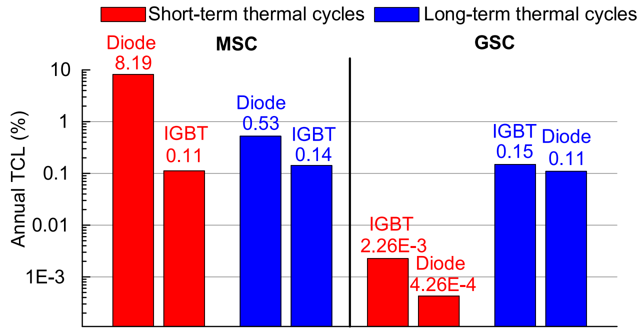

Fig. 13. Annual total consumed lifetimes (TCLs) comparison of diode and IGBT with different thermal cycles.

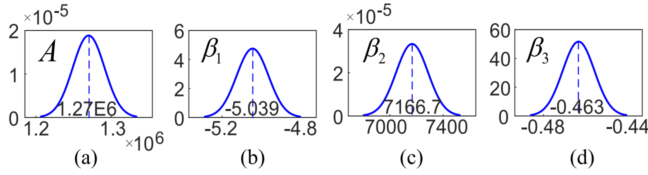

Fig. 14. Normal PDFs for coefficients in Bayerer's lifetime model (a) A, (b) β_1, (c) β_2, and (d) β_3.

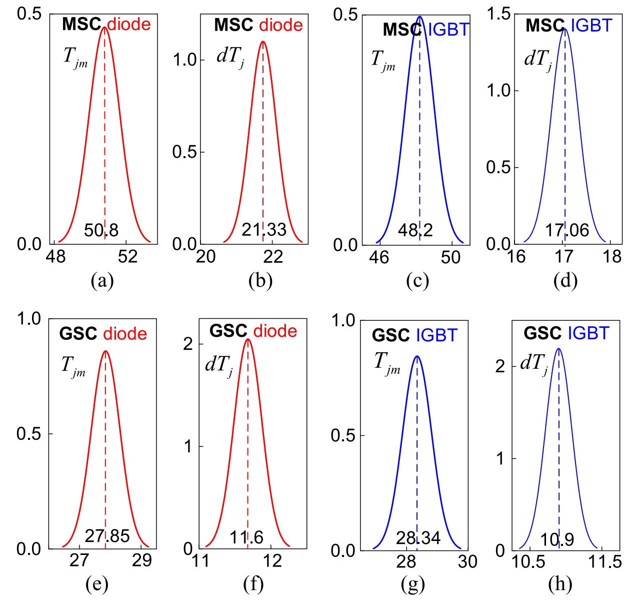

Fig. 15. Normal PDFs for thermal stress related parameters in Bayerer's lifetime model: (a) mean junction temperature and (b) junction temperature fluctuation for diode in MSC; (c) mean junction temperature and (d) junction temperature fluctuation for IGBT in MSC; (e) mean junction temperature and (f) junction temperature fluctuation for diode in GSC; (g) mean junction temperature; and (h) junction temperature fluctuation for IGBT in GSC.

Bayerer's lifetime model should be taken into consideration:

$$N_{f_\text{diode/IGBT}} = A \cdot dT_{j_\text{diode/IGBT}}^{\beta_1} \cdot e^{\left(\frac{\beta_2}{T_{jm_\text{diode/IGBT}}+273}\right)} \cdot t_{\text{on}}^{\beta_3}. \quad (9)$$

For Bayerer's lifetime formula in (9), N_f represents the power cycles to failure, A, β_1, β_2, and β_3 are provided by the manufacturer of the semiconductors according to the power cycle test data [38], [39]. Although all these coefficients are statistically fitted and chosen as constants to simplify the calculation, uncertainties for these parameters still exist [24]. It is assumed that all of these coefficients are under a standard normal distribution and have 5% variations to their center values; thus, the probability density functions (PDFs) of A to β_3 are shown as Fig. 14. For the thermal stress related parameters mean junction temperature T_{jm} and junction temperature fluctuation dT_j in Bayerer's lifetime model, variations are induced by the uncertainties of maximum or minimum semiconductor ON-state resistances during the manufacturing process. Normal distributions with 5% variations are also applied to describe temperature-related parameters in diode and IGBT for both the MSC and GSC, which are illustrated in Fig. 15.

Taking variations of all parameters into account, a 10 000 sampling Monte Carlo method can be utilized to analyze the failure and lifetime distributions for diode and IGBT. In the MSC, the annual damage for one semiconductor component can be obtained by adding its TCLs under long-term thermal cycles and short-term thermal cycles. While for the GSC, as the short-term thermal cycle based TCL is several orders of magnitude lower than those under long-term thermal cycles, only the TCL of 1.5E-4 for the IGBT and 1.1E-4 for the diode are considered. Moreover, Weibull distributions are used to fit the damage and time-to-failure (reciprocal of the damage rate) data for power semiconductors [40]:

$$f(x) = \frac{\beta}{\lambda}\left(\frac{x}{\lambda}\right)^{\beta-1} e^{-\left(\frac{x}{\lambda}\right)^{\beta-1}} \quad (10)$$

where f denotes the PDF, λ and β are, respectively, the scale and shape parameters of the profile.

As illustrated in Figs. 16 and 17, the unreliability cumulative distribution functions for diode and IGBT are obtained by accumulating their damage PDFs. It can be observed that the diode in the MSC has the lowest B_1 lifetime, which is 30 years, while this number is 114 years for the IGBT in MSC. For the GSC, the diode and IGBT both have much lower unreliable probabilities comparing with those in the MSC, which is accordance with the thermal stress results reflected in Fig. 13. According to [4], the lowest B_1 lifetime for components in the BTB converter of this research is still highly over the engineering recommendations, which proves the design reasonability of the proposed wind power system.

VI. Parameter Sensitivity Analysis in the Bayerer's Lifetime Model

As indicated in Section V, the numerical Monte Carlo algorithm is utilized under the condition of assuming a 5% uncertainty for all parameters in the Bayerer's lifetime model. However, there is no explicit criterion for the selection of this deviation. Although the 5% has been adopted by numerous state-of-the-art researches, it still requires a deeper investigation. In this section, analysis is mainly focused in the MSC, all of the dimensionless coefficients A, β_1, β_2, and β_3 and the temperature-related parameters T_{jm}, dT_j in the Bayerer's lifetime model are assumed having a set of standard deviations

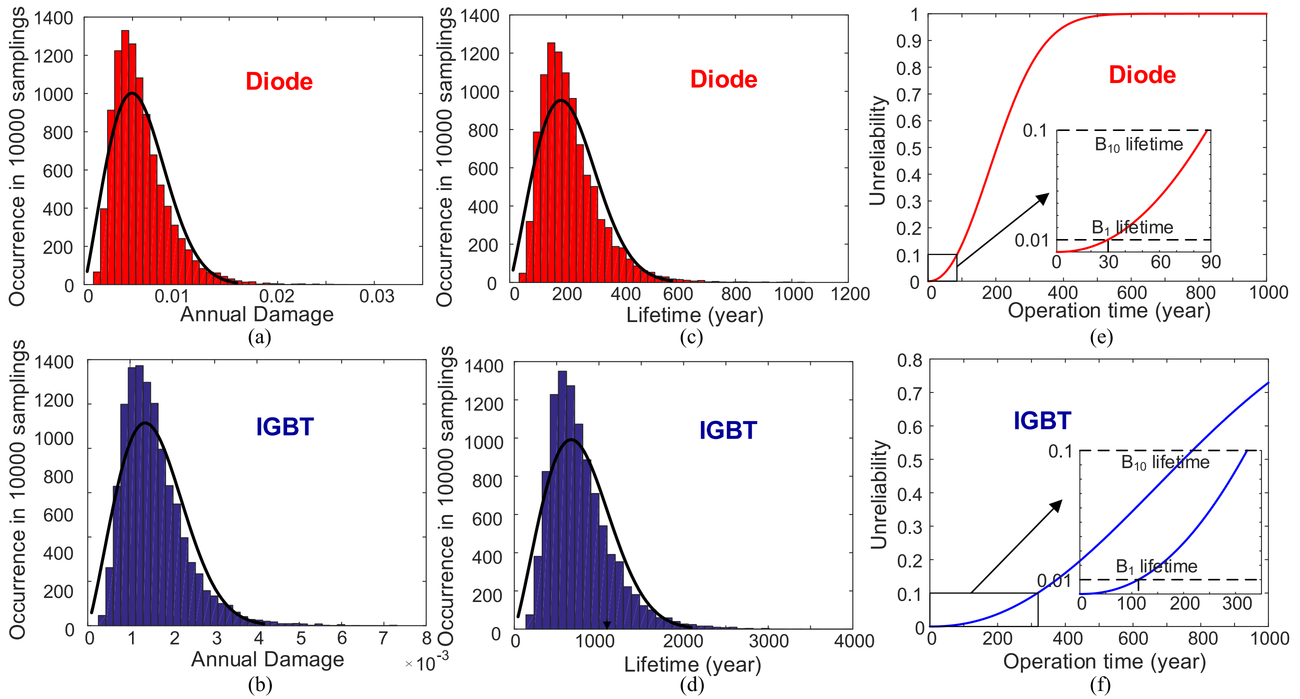

Fig. 16. Monte Carlo analysis results for MSC: annual damage Weibull distributions for (a) diode and (b) IGBT; lifetime Weibull distributions for (c) diode and (d) IGBT; unreliability profiles for (e) diode and (f) IGBT.

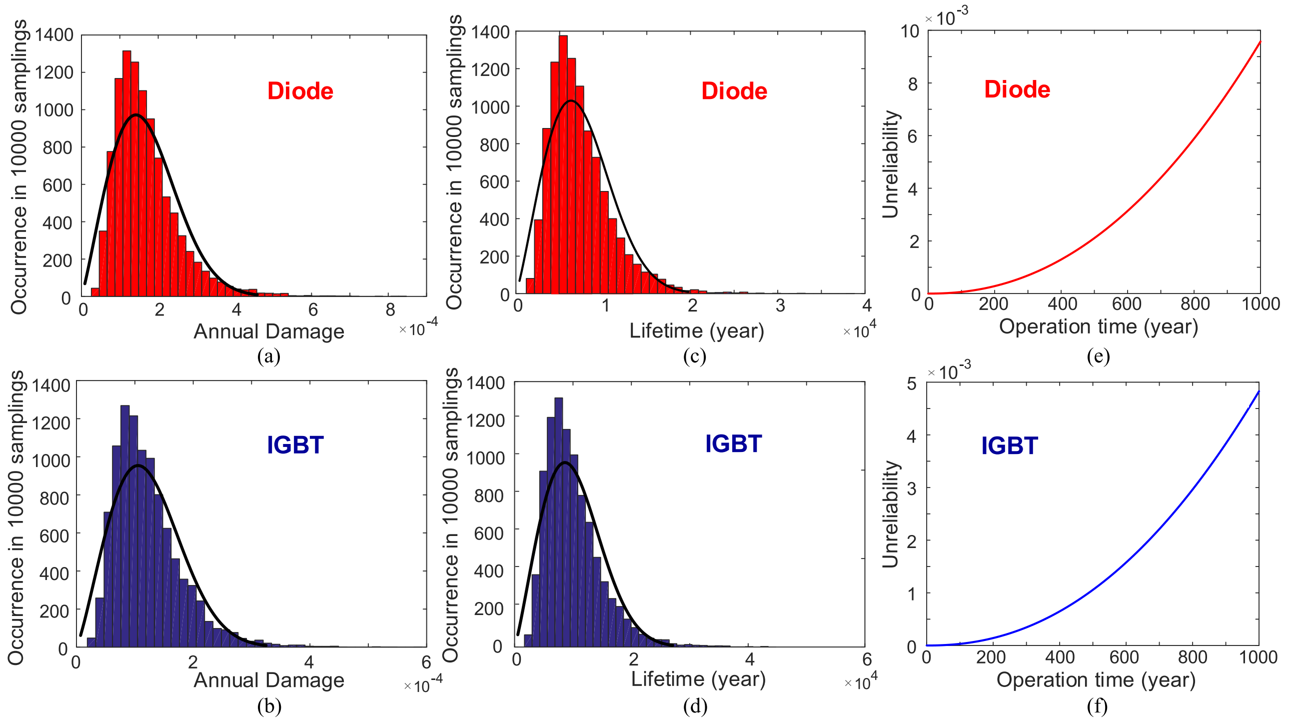

Fig. 17. Monte Carlo analysis results for GSC: annual damage Weibull distributions for (a) diode and (b) IGBT; lifetime Weibull distributions for (c) diode and (d) IGBT; unreliability profiles for (e) diode and (f) IGBT.

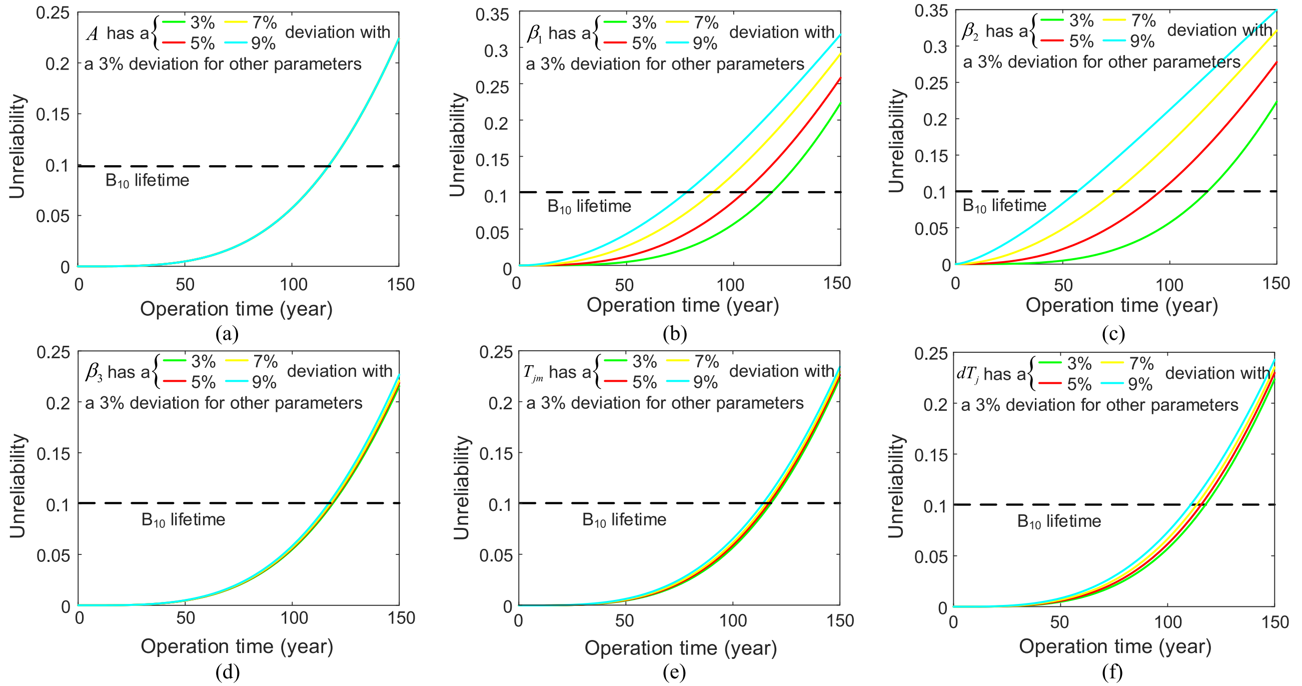

Fig. 18. Parameter sensitivity of (a) A, (b) β_1, (c) β_2, (d) β_3, (e) T_{jm}, and (f) dT_j in the Bayerer's lifetime model from the diode reliability point of view.

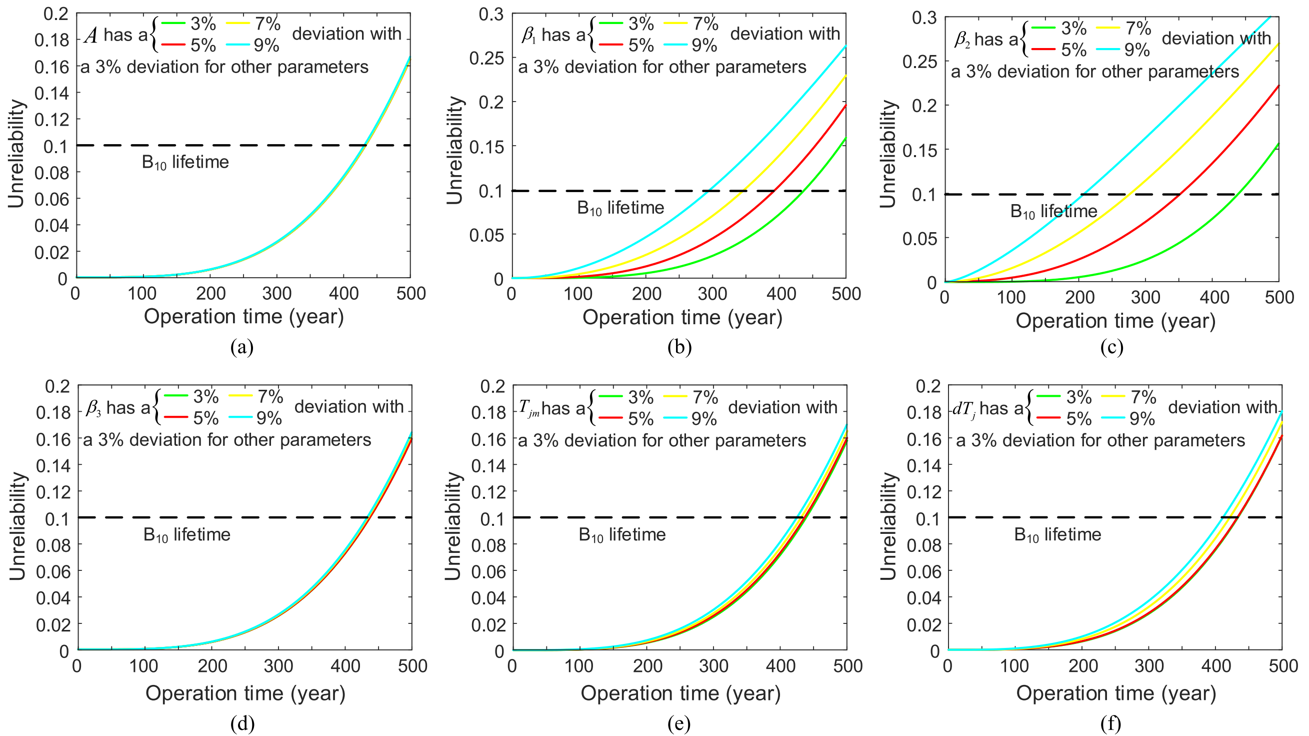

Fig. 19. Parameter sensitivity of (a) A, (b) β_1, (c) β_2, (d) β_3, (e) T_{jm}, and (f) dT_j in the Bayerer's lifetime model from the IGBT reliability point of view.

of 3%, 5%, 7%, and 9% for their normal distributions. By remaining deviation of other parameters as 3% and changing the deviation of one parameter in sequence from 3% to 9%, different component reliability profiles can be obtained via paralleled Monte Carlo methods. Subsequently, influence of different deviations to the semiconductor lifetime and the sensitivity of the selected parameter can be analyzed from the reliability point of view. Figs. 18 and 19 illustrate lifetime difference induced by each parameter deviations of diode and IGBT, respectively.

It is observed from Fig. 18, parameter sensitivity to the diode reliability is quantitatively revealed by the B_{10} lifetime difference. For parameters A, β_3, T_{jm}, and dT_j, when their

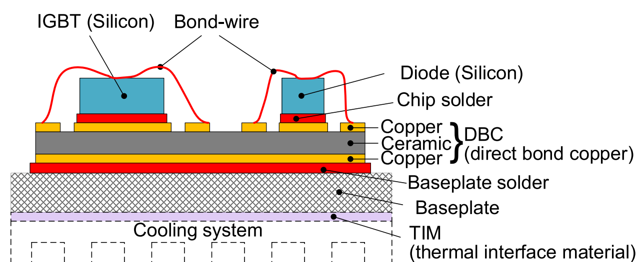

Fig. 20. Typical configuration layout for semiconductors.

normal deviations vary from 3% to 9%, the corresponding B_{10} lifetimes all have no more than 6.8% fluctuation, which is sufficiently small to be neglected in an engineering level. However, large lifetime fluctuations emerge under the β_1 and β_2 deviation changing, for coefficient β_1, a 35.6% B_{10} lifetime decrease occurs when its normal deviation increases from 3% (B_{10} lifetime: 119.2 years) to 9% (B_{10} lifetime: 76.8 years), while for coefficient β_2, the lifetime decrease is 54% (from 117.8 years under 3% deviation to 54.2 years under 9% deviation). Similar phenomena can also be revealed by the IGBT B_{10} lifetime in Fig. 19, parameters A, β_3, T_{jm}, and dT_j also have lower sensitivity to the IGBT reliability, while non-negligible 34.6% (from 431.8 years under 3% deviation to 282.3 years under 9% deviation) and 53.1% (from 429.7 years under 3% deviation to 201.5 years under 9% deviation) B_{10} lifetime decreases occur under coefficients β_1 and β_2 deviation changing, respectively.

By taking the logarithm for both sides of the Bayerer's lifetime equation, it can be found that β_1 and β_2 are coefficients of the temperature-related parameters dT_j and T_{jm}, respectively. According to [24], [41], these two coefficients are fitted based on numerous fast power cycle tests, and they highly depend on the material properties of the power semiconductor module, such as the coefficient of thermal expansion, the Young's modulus, and the yield strength. Generally, a typical layout of the semiconductor power module is illustrated in Fig. 20 [42]. The semiconductor die is welded and connected onto the direct bonding copper (DBC) via the solder.

Connection with different die chips and copper terminal are achieved by using the bond-wire. The DBC is usually designed as the copper–ceramic–copper or the copper–Al_2O_3–copper three-layer structure to perform as an electric isolator. The other side of the DBC is welded on a baseplate with the aid of the baseplate solder to generate a seven-layer semiconductor module layout. Obviously, the material type and thickness for each layers influence their properties, and subsequently β_1 and β_2 in the lifetime calculation of the entire semiconductor module. Therefore, it is essential to adjust the center values of parameters in the Bayerer's lifetime model, especially β_1 and β_2, according to a new group of accelerated power cycling test result for different semiconductor configurations.

VII. Conclusion

This article has presented a reliability comparison for semiconductors between different thermal cycles and evaluated the component-level reliability for a direct-drive PMSG-based BTB converter. First, TCLs for diode and IGBT under long-term thermal cycles and short-term thermal cycles are obtained separately and compared. Experimental results reveal the thermal stresses of the diode and IGBT under different converter operation modes. Then, based on the Bayerer's lifetime model and the Monte Carlo method, the overall component-level reliability of the BTB converter is analyzed. It is observed that B_1 lifetime for power components in the proposed system fulfill the industry requirement. Finally, sensitivities of parameters in the Bayerer's lifetime formula are analyzed from the B_{10} lifetime point of view, it is concluded that coefficients β_1 and β_2 are sensitive to the deviation changing. For different power semiconductor configurations, slight adjustments should be considered to the Bayerer's lifetime model.

References

[1] F. Blaabjerg and K. Ma, "Future on power electronics for wind turbine systems," *IEEE Trans. Emerg. Sel. Topics Power Electron.*, vol. 1, no. 3, pp. 139–152, Sep. 2013.

[2] H. Wang and F. Blaabjerg, "Power electronics reliability: State of the art and outlook," *J. Emerg. Sel. Topics Power Electron.*, to be published, doi: 10.1109/JESTPE.2020.3037161.

[3] M. Tsili and S. Papathanassiou, "A review of grid code technical requirements for wind farms," *IET Renewable Power Gener.*, vol. 3, no. 3. pp. 308–332, Sep. 2009.

[4] H. Wang, K. Ma, and F. Blaabjerg, "Design for reliability of power electronic systems," in *Proc. 38th Annu. Conf. IEEE Ind. Electron. Soc.*, 2012, pp. 33–44.

[5] J. Falck, C. Felgemacher, A. Rojko, M. Liserre, and P. Zacharias, "Reliability of power electronic systems: An industry perspective," *IEEE Ind. Electron. Mag.*, vol. 12, no. 2, pp. 24–35, Jun. 2018.

[6] K. Ma, M. Liserre, F. Blaabjerg, and T. Kerekes, "Thermal loading and lifetime estimation for power device considering mission profiles in wind power converter," *IEEE Trans. Power Electron.*, vol. 30, no. 2, pp. 590–602, Feb. 2015.

[7] K. Fischer *et al.*, "Exploring the causes of power-converter failure in wind turbines based on comprehensive field-data and damage analysis, " *Energies*, vol. 12, 2019, Art. no. 593.

[8] K. Fischer *et al.*, "Reliability of power converters in wind turbines: Exploratory analysis of failure and operating data from a worldwide turbine fleet," *IEEE Trans. Power Electron.*, vol. 34, no. 7, pp. 6332–6344, Jul. 2019.

[9] D. Zhou and F. Blaabjerg, "Converter-level reliability of wind turbine with low sample rate mission profile," *IEEE Trans. Ind. Appl.*, vol. 56, no. 3, pp. 2938–2944, May/Jun. 2020.

[10] Q. Zhou, S. Xue, J. Li, C. Xiang, and S. Chen, "Evaluation of wind power converter reliability considering multi-time scale and mission profiles," in *Proc. IEEE Int. Conf. High Voltage Eng. Appl.*, 2016, pp. 1–4.

[11] C. Olmi, F. Sculler, and J. Charpentier, "Impact of input data scattering on the reliability function of a wind turbine power electronic converter," in *Proc. IEEE Int. Power Electron. Appl. Conf. Expo.*, 2018, pp. 1–6.

[12] F. Feng *et al.*, "Operational reliability model of hybrid MMC considering multiple time scales and multi-state submodule," *J. Modern Power Syst. Clean Energy*, to be published, doi: 10.35833/MPCE.2019.000227.

[13] G. Zhang, D. Zhou, F. Blaabjerg, and J. Yang, "Mission profile resolution effects on lifetime estimation of doubly-fed induction generator power converter," in *Proc. IEEE Southern Power Electron. Conf.*, 2017, pp. 1–6.

[14] C. Smith, C. Crabtree, and P. Matthews, "Impact of wind conditions on thermal loading of PMSG wind turbine power converters," *IET Power Electron.*, vol. 10, no. 11, pp. 1268–1278, Sep. 2017.

[15] E. Baygildina, P. Peltoniemi, O. Pyrhönen, K. Ma, and F. Blaabjerg, "Thermal loading of wind power converter considering dynamics of wind speed," in *Proc. 39th Annu. Conf. IEEE Ind. Electron. Soc.*, 2013, pp. 1362–1367.

[16] R. Pittini, S. D'Arco, M. Hernes, and A. Petterteig, "Thermal stress analysis of IGBT modules in VSCs for PMSG in large offshore wind energy conversion systems," in *Proc. 14th Eur. Conf. Power Electron. Appl.*, 2011, pp. 1–10.

[17] D. Zhou, F. Blaabjerg, M. Lau, and M. Tonnes, “Comparison of wind power converter reliability with low-speed and medium-speed permanent-magnet synchronous generators,” *IEEE Trans. Ind. Electron.*, vol. 62, no. 10, pp. 6575–6584, Oct. 2015.

[18] D. Zhou, G. Zhang, and F. Blaabjerg, “Optimal selection of power converter in DFIG wind turbine with enhanced system-level reliability,” *IEEE Trans. Ind. Appl.*, vol. 54, no. 4, pp. 3637–3644, Jul./Aug. 2018.

[19] A. Isidori, F. M. Rossi, F. Blaabjerg, and K. Ma, “Thermal loading and reliability of 10-MW multilevel wind power converter at different wind roughness classes,” *IEEE Trans. Ind. Appl.*, vol. 50, no. 1, pp. 484–494, Jan./Feb. 2014.

[20] Military Handbook, Reliability Prediction of Electronic Equipment, Standard MIL-HDBK-217F, Dec. 1991.

[21] J. Harms, Revision of MIL-HDBK-217, Reliability Prediction of Electronic Equipment, 2010.

[22] Y. Zhang, H. Wang, Z. Wang, Y. Yang, and F. Blaabjerg, “Impact of the thermal-interface-material thickness on IGBT module reliability in the modular multilevel converter,” in *Proc. Int. Power Electron. Conf. IPEC-Niigata*, 2018, pp. 2743–2749.

[23] P. D. T. O’Connor and A. Kleyner, *Practical Reliability Engineering*, 5th ed. New York, NY, USA: Wiley, 2012.

[24] R. Bayerer, T. Herrmann, T. Licht, J. Lutz, and M. Feller, “Model for power cycling lifetime of IGBT modules—Various factors influencing lifetime,” in *Proc. 5th Int. Conf. Integr. Power Electron. Syst.*, Mar. 2008, pp. 1–6.

[25] A. Wintrich, N. Ulrich, T. Werner, and T. Reimann, *Application Manual Power Semiconductors*. Nuremberg, Germany: Semikron Int.GmbH, 2015.

[26] Z. Qin, W. Li, and X. Xiong, “Generation system reliability evaluation incorporating correlations of wind speeds with different distributions,” *IEEE Trans. Power Syst.*, vol. 28, no. 1, pp. 551–558, Feb. 2013.

[27] D. Zhou, H. Wang, and F. Blaabjerg, “Mission profile based system-level reliability analysis of DC/DC converters for a backup power application,” *IEEE Trans. Power Electron.*, vol. 33, no. 9, pp. 8030–8039, Sep. 2018.

[28] H. Wang, P. Davari, H. Wang, D. Kumar, F. Zare, and F. Blaabjerg, “Lifetime estimation of DC-Link capacitors in adjustable speed drives under grid voltage unbalances,” *IEEE Trans. Power Electron.*, vol. 34, no. 5, pp. 4064–4078, May 2019.

[29] “Enercon E-82 wind turbine,” Enercon, Aurich, Germany. 2016. [Online]. Available: https://www.enercon.de/en/products/ep-2/e-82/

[30] B. Wu, Y. Lang, N. Zargari, and S. Kouro, *Power Conversion and Control of Wind Energy Systems*. Piscataway, NJ, USA: Wiley, 2011.

[31] ABB Application Notes: Applying IGBTs, Apr. 2009, pp. 22–23.

[32] R. Schnell, M. Bayerer, and S. Geissmann, “Thermal design and temperature ratings of IGBT modules,” ASEA Brown Boveri, Zurich, Switzerland, ABB Application Note, 5SYA 2093-00, 2011.

[33] Z. Ni, X. Lyu, O. P. Yadav, B. N. Singh, S. Zheng, and D. Cao, “Overview of real-time lifetime prediction and extension for SiC power converters,” *IEEE Trans. Power Electron.*, vol. 35, no. 8, pp. 7765–7794, Aug. 2020.

[34] D. Zhou, F. Blaabjerg, M. Lau, and M. Tonnes, “Thermal profile analysis of doubly-fed induction generator based wind power converter with air and liquid cooling methods,” in *Proc. 15th Eur. Conf. Power Electron. Appl.*, 2013, pp. 1–10.

[35] M. A. Miner, “Cumulative damage in fatigue,” *J. Appl. Mech.*, vol. 12, pp. A159–A164, 1945.

[36] D. Zhou, Y. Peng, F. Iannuzzo, M. Hartmann, and F. Blaabjerg, “Thermal mapping of power semiconductors in H-bridge circuit,” *Appl. Sci.*, vol. 10, 2020, Art. no. 4340.

[37] OTG-F Fiber Optic Temperature Sensor. 2021. [Online]. Available: https://opsens-solutions.com/products/fiber-optictemperature-sensors

[38] B. Gao, F. Yang, M. Chen, Y. Chen, W. Lai, and C. Liu, “Thermal lifetime estimation method of IGBT module considering solder fatigue damage feedback loop,” *Microelectron. Rel.*, vol. 82, pp. 51–61, Mar. 2018.

[39] G. Zhang, D. Zhou, J. Yang, and F. Blaabjerg, “Fundamental-frequency and load-varying thermal cycles effects on lifetime estimation of DFIG power converter,” *Microelectron. Rel.*, vol. 76–77, pp. 549–555, Sep. 2017.

[40] “Life data analysis reference,” ReliaSoft Corporation, 2015. [Online]. Available: http://reliawiki.org/index.php/Life_Data_Analysis_Reference_Book

[41] M. Held, P. Jacob, G. Nicoletti, P. Scacco, and M. H. Poech, “Fast power cycling test for IGBT modules in traction application,” in *Proc. 2nd Int. Conf. Power Electron. Drive Syst.*, 1997, pp. 425–430.

[42] B. Ji, X. Song, E. Sciberras, W. Cao, Y. Hu, and V. Pickert, “Multiobjective design optimization of IGBT power modules considering power cycling and thermal cycling,” *IEEE Trans. Power Electron.*, vol. 30, no. 5, pp. 2493–2504, May 2015.